Theoretical investigations of the vortex lattice and de Haas-van Alphen oscillations in the superconducting state

Theoretical investigations of the vortex lattice and de Haas–van Alphen oscillations in the superconducting state

P Miller and B L Györffy

H H Wills Physics Laboratory, University of Bristol, Tyndall Avenue, Bristol BS8 1TL, UK

Abstract. After initial calculations for a single vortex, where the Bogoliubov–de Gennes equations, corresponding to a simple tight-binding model, are solved using the recursion method, a fully self-consistent microscopic solution for the Abrikosov flux lattice is given. In the case of the latter, the observation of discrete Landau-like levels with a large order parameter suggests a form for the energy spectrum which can give rise to oscillations of the thermodynamic potential as the magnetic field varies, even when there are no normal electrons in the system. These de Haas–van Alphen oscillations are studied analytically following a generalized version of the Lifshitz–Kosevich argument, and it is found that their amplitude in the superconducting state is damped compared with what they would have been in the normal state. These results are supported by further, approximate, computations.

1. Introduction

The nature of the vortex state (or Abrikosov flux lattice) in type II superconductors was discovered by Abrikosov in 1957 [1] on the basis of Ginzburg–Landau theory, but a fully microscopic theory of this very complex phenomenon has become of interest only recently [2, 3, 4, 5, 6]. In this paper, we report on our investigations of the problem by solving the Bogoliubov–de Gennes equations in a magnetic field, using a real space method. The current interest in obtaining a fuller theoretical understanding of the mixed state has been spurred on by the observation of de Haas–van Alphen oscillations in superconducting samples [7, 8, 9, 10]. We hope to shed some light on these experimental findings, by studying the local quasiparticle density of states for a simple model.

The problem to be solved is formulated as a tight-binding Bogoliubov–de Gennes equation, for the particle and hole local amplitudes u_i^λ and v_i^λ respectively. For the eigensolutions labelled by λ, this is given by

$$\sum_j \begin{pmatrix} \varepsilon_i \delta_{ij} + t_{ij} & \Delta_i \delta_{ij} \\ \Delta_i^* \delta_{ij} & -\varepsilon_i \delta_{ij} - t_{ij}^* \end{pmatrix} \begin{pmatrix} u_j^\lambda \\ v_j^\lambda \end{pmatrix} = E_\lambda \begin{pmatrix} u_i^\lambda \\ v_i^\lambda \end{pmatrix} \tag{1}$$

where $\varepsilon_i = [Un_i/2 + \epsilon_0 - \mu]$ is the total 'on-site energy', the hopping integral, t_{ij}, does not include the on-site term, $t_{ii} = \epsilon_0$, U is the electron–electron coupling energy, n_i is the local electron number and μ is the chemical potential. The above equation can be derived from a negative-U Hubbard model, via the Hartree–Fock–Gor'kov decoupling method [11]. The

magnetic field enters the Hamiltonian through a vector potential in a Peierls phase of the hopping integral,

$$t_{ij} \mapsto t_{ij} \exp \left\{ \frac{-\mathrm{i}e}{\hbar} \int_{r_i}^{r_j} A(r') \cdot dr' \right\} = t_{ij} \, \mathrm{e}^{-\mathrm{i}A_{ij}}. \tag{2}$$

The system is solved using the recursion method [12, 13, 14], which is a natural real space procedure for inhomogeneous tight-binding problems, adapted to study superconductivity in a magnetic field [15]. A self-consistent solution is found for the electron number, n_i, and order parameter, Δ_i, on each site of a square lattice, as well as the fluxes through plaquettes of size $a \times a$ from currents, and hence vector potentials along links. The latter involves use of a discretized form of Maxwell's equations, described in appendix A.

In the formalism of the recursion method [12, 13, 14] then, the local electron number for the ith site is found with a starting state, $\left| \psi_0^A \right\rangle = |u_i\rangle$, where $|u_i\rangle$ corresponds to the orbital associated with site i. As it turns out, the local electron number is given by

$$n_i = \int_{-\infty}^{\infty} n_i^u(\varepsilon) f(\varepsilon) = \frac{-2}{\pi} \mathrm{Im} \left[\int_{-\infty}^{\infty} G_{ii}^{uu}(\varepsilon + \mathrm{i}\eta) f(\varepsilon) \, d\varepsilon \right] \tag{3}$$

where the Green function, $G_{ii}^{uu}(\varepsilon + \mathrm{i}\eta)$, is the one calculated using the continued fraction representation of the recursion method, with the above starting state, and $f(\varepsilon)$ is the usual Fermi–Dirac distribution. The function $n_i^u(\varepsilon)$, implicitly defined in the above equation, will be referred to as the local particle density of states later.

Continuing, to find the order parameter the recursion starts with the states $\left| \psi_0^B \right\rangle = |v_i\rangle$, $\left| \psi_0^C \right\rangle = (1/\sqrt{2}) |u_i + v_i\rangle$, and $\left| \psi_0^D \right\rangle = (1/\sqrt{2}) |u_i + \mathrm{i}v_i\rangle$, and yields the Green functions $G_{ii}^B(\varepsilon)$, $G_{ii}^C(\varepsilon)$, and $G_{ii}^D(\varepsilon)$. Following the arguments in [12], the Green function required to calculate the order parameter is found to be

$$G_{ii}^{vu}(\varepsilon) = \frac{1}{2} \mathrm{Re} \left[G_{ii}^C(\varepsilon) - G_{ii}^A(\varepsilon) - G_{ii}^B(\varepsilon) \right] + \frac{\mathrm{i}}{2} \mathrm{Im} \left[G_{ii}^D(\varepsilon) - G_{ii}^A(\varepsilon) - G_{ii}^B(\varepsilon) \right] \tag{4}$$

and the calculation proceeds via the usual formula

$$\Delta_i = -U \frac{-1}{\pi} \mathrm{Im} \left[\int_{-\infty}^{\infty} G_{ii}^{vu}(\varepsilon + \mathrm{i}\eta) \left[1 - 2f(\varepsilon) \right] d\varepsilon \right]. \tag{5}$$

Similarly, the currents can be calculated, with the following choices of starting states: $\left| \psi_0^E \right\rangle = (1/\sqrt{2}) |u_i + \mathrm{i}\, \mathrm{e}^{-\mathrm{i}A_{ij}} u_j\rangle$ and $\left| \psi_0^F \right\rangle = (1/\sqrt{2}) |u_i - \mathrm{i}\, \mathrm{e}^{-\mathrm{i}A_{ij}} u_j\rangle$. In this case, the required Green function is

$$\mathrm{Im} \left[\mathrm{e}^{-\mathrm{i}A_{ij}} G_{ij}^{uu}(\varepsilon) \right] = \tfrac{1}{2} \left[G_{ij}^F(\varepsilon) - G_{ij}^E(\varepsilon) \right] \tag{6}$$

and it allows the currents to be calculated from

$$\begin{aligned}
I_{ij} &= \int_{-\infty}^{\infty} I_{ij}(\varepsilon) f(\varepsilon) \\
&= \frac{-2}{\pi} \mathrm{Im} \left\{ \int_{-\infty}^{\infty} \left[\mathrm{i}\, \mathrm{e}^{-\mathrm{i}A_{ij}} G_{ij}^{uu}(\varepsilon + \mathrm{i}\eta) - \mathrm{i}\, \mathrm{e}^{\mathrm{i}A_{ij}} G_{ij}^{uu*}(\varepsilon + \mathrm{i}\eta) \right] f(\varepsilon) \, d\varepsilon \right\}.
\end{aligned} \tag{7}$$

Clearly the function $I_{ij}(\varepsilon)$ is the current distribution in energy.

The computations by the recursion method involved a highly parallelized code. The same method and parallel computer were used for the flux lattice solution as well as the single-vortex problem, so the following description applies to both. With such real space lattice calculations, a unique lattice site can be associated with each node (processor) of the parallel computer. The recursion method is carried out on each node concurrently, each with

its unique lattice site as the first basis state. The same method is followed by all the nodes, and the electron number, n_i, order parameter, Δ_i, and two link currents, I_{ij}, from a site are found independently on each node. The data are combined, so that the new parameters for all lattice sites and the two-dimensional array of links is updated together. One node is specifically assigned to carry out the iteration procedure and to pass the new starting set of parameters back to the others, until self-consistency is achieved.

All calculations were carried out at zero temperature ($T = 0$) and with a large inter-action energy of $U = -6t$. These parameters were chosen for computational convenience. Working at zero temperature is an advantage, as the sum over the Matsubara-like poles on the semicircle [16, 15] is much more rapidly evaluated by a Gaussian–Legendre integral method [17], which corresponds to zero spacing between poles. The large value of the interaction energy was necessary in order to obtain reasonably accurate solutions. A stringent test of the accuracy of a self-consistent solution is the requirement that the sum of currents flowing along links towards any particular site must be zero. When the above choice of parameters was used, all the currents cancelled by better than one part in 10^6, so one can have confidence in the accuracy of the solutions.

2. The single vortex

As a preliminary to calculations for the vortex lattice by the recursion method, we used it to investigate a single vortex in the superconducting state. Like the negative-U impurity problem [15], study of a single vortex is ideally suited to display the power of the recursion method. There is no translational periodicity in the problem, and it is essentially a local perturbation in real space. Nevertheless, the physical consequences for the vector potential and phase of the order parameter extend through all space, which severely challenges the numerical efficiency of the method.

Much previous work has been done on the isolated vortex problem [18, 19, 20, 21]. Approaches using Ginzburg–Landau theory and quasiclassical theory as well as solutions of the Bogoliubov–de Gennes equations by expansions in angular momentum states have been deployed to good effect. Results presented here both fit in with and add to this framework of previous results.

The full set of quantities of interest in the vortex state also requires self-consistent calculation in the case of a single vortex. The real and imaginary parts of the order parameters, electron numbers, currents, fields, and vector potentials must all be obtained self-consistently, through all space. Of course, to render the problem tractable we shall seek self-consistent solutions only for a finite region of space and match these to approximate solutions on the outside. Note that termination of the recursion method after a finite number of steps means that distant sites do not effect the solution at the vortex centre on a particular iteration, but any errors do move into the centre as the iteration continues. The Ginzburg–Landau solution was chosen then to act as a boundary to the self-consistent region. Therefore, the recursion method was used for a relatively small number of sites around the vortex centre. The linear size of this central region was much larger than the coherence length, ξ_0, but much less than the penetration depth, λ. Hence the details of the order parameter do match very well between the self-consistent region and the Ginzburg–Landau region, but the currents and vector potentials can show some discontinuity. Consequently, more confidence should be placed in the structure of the order parameter found at the vortex centre than in values of the magnetic field. To obtain the correct flux quantization, self-consistency calculations would need to be carried out up to distances greater than the penetration depth, where the circulating current tends to zero. This was not done in these calculations.

The Ginzburg–Landau solution for the magnetic induction, B, which is used in the first iteration for the field variation, and is always kept for large radius, is given by the zeroth-order Bessel function of imaginary argument, $K_0(r)$:

$$B(x, y) = \frac{\phi_{0,s}}{2\pi\lambda^2} K_0\left(\frac{r}{\lambda}\right) \tag{8}$$

where, of course, r is the distance from the vortex centre at $(0, 0)$. Asymptotically, the function has the form [22]

$$\lim_{r \to \infty} (B(r)) \approx \frac{\phi_{0,s}\sqrt{\lambda}}{2\sqrt{2\pi r}\lambda^2} \exp\left[-\frac{r}{\lambda}\right]. \tag{9}$$

The above form gives the field variation as a continuous function of r. To make use of it in the lattice model, the distance to the vortex line, r, is calculated from the centre of each plaquette. Multiplication by a^2 gives the flux through the plaquette. A parameter in the theory is the penetration depth, λ, which is taken hereafter to be a 100 lattice spacings ($\lambda = 100a$).

All calculations, whether for a single vortex or a flux lattice, were performed on a square lattice of sites, and only solutions which maintained a square symmetry were sought and found. A great deal of time was saved by making best use of the C_{4v} symmetry. Only the quantities associated with one octant of the square unit cell need to be calculated, as all sites within the square are related to a site within the octant by a symmetry operation. The geometrical symmetry of the Hamiltonian, which is not further broken in our solutions, means that the electron number, and magnitudes of the order parameter and link currents, are the same on sites related by symmetry. Care must be taken with the phase of the order parameter and value of link vector potentials, but a simple choice of gauge maintains the symmetry.

It should be noted that the problem is solved in two dimensions only. Practical considerations of computational time force such a limitation on the calculations. Any qualitative effects are expected to be present, as the symmetry of the problem is two dimensional. The significant effect of the motion in the direction of vortices is to spread discrete states into cosine bands. The above points are true for the vortex lattice as well as the single-vortex calculations.

A full solution of the single-vortex problem was carried out on 128 nodes, so a self-consistent determination of the various quantities such as electron number and order parameter was made for sites up to 15 lattice spacings from the central site in the $(1, 0)$ directions, and 14 diagonal spacings (of $\sqrt{2}a$) in the $(1,1)$ directions.

The variations of the order parameter, and distribution of currents and fields, are similar to those for one unit cell of the flux lattice, to be discussed later in connection with figures 5–7. The results are taken in the symmetrical case of half filling, so the electron number is the same on each site. It is apparent that with such a large value of $-U/t$, which leads to a large value of the order parameter ($\Delta \approx 2.5t$), the coherence length is of the order of the lattice spacing—the order parameter approaches its full magnitude on sites neighbouring the central site where it is zero. The anticlockwise circulating currents are seen to be a maximum only one lattice spacing from the vortex core site, close to a coherence length from the centre, as expected.

As part of our general strategy for studying the quasiparticle spectra of an inhomogeneous state, we have calculated the local particle density of states, defined by

$$n_0^e(\varepsilon, r_i) = \sum_{\lambda} \frac{|u_i^\lambda|^2}{\varepsilon + i\eta - E_\lambda}. \tag{10}$$

For a number of different sites our results are displayed in figure 1. In connection with them there are several remarks in order. Firstly, the main band of states does not reveal Landau quantized levels, as one might have expected. Due to the small magnetic field, their spacing would be too small to be resolved using the present method. Secondly, there is a state at zero energy (i.e. lying at the chemical potential), whose main amplitude is on the central, normal site. This is a localized state, first discussed by Bardeen and coworkers [23], whose amplitude falls rapidly away from the central site, within a few lattice spacings.
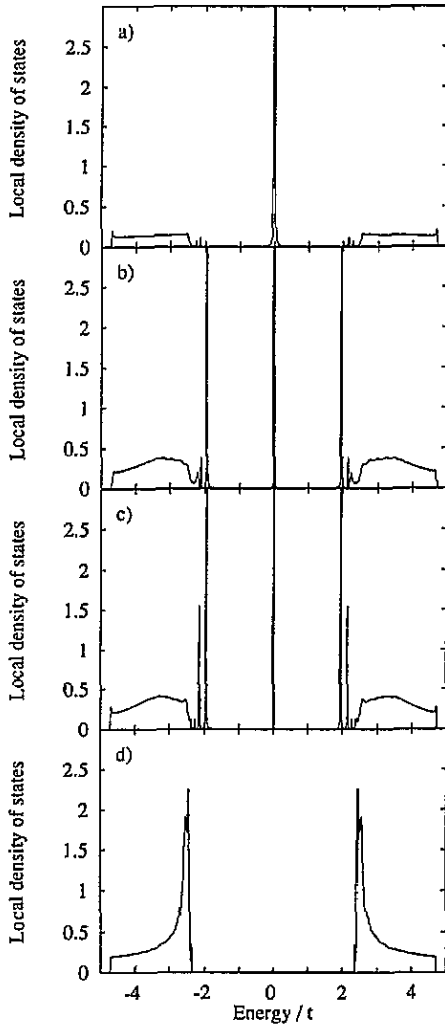
Figure 1. Local densities of states for a single vortex on the following sites: (a) site (0, 0); (b) site (1, 0); (c) site (1, 1); and (d) site (15, 0), where (0, 0) is the central site of the vortex.
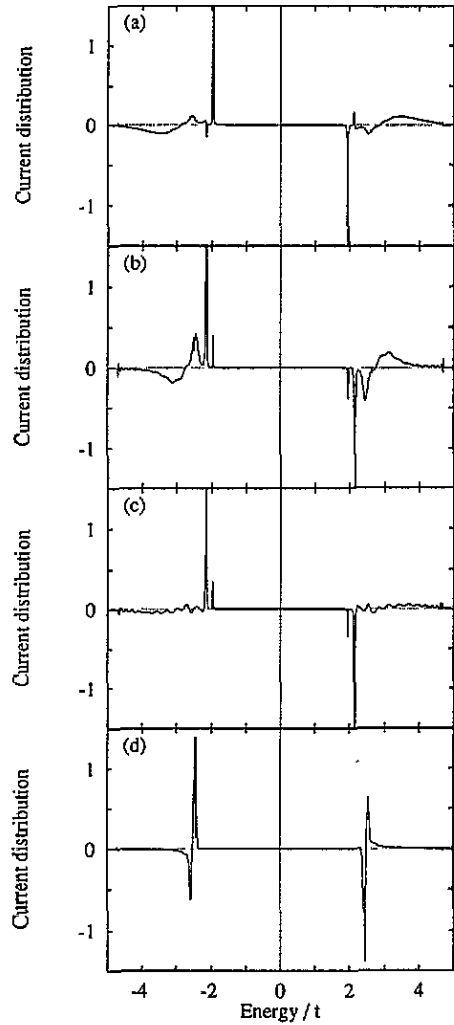
Figure 2. y current carrying distribution in energy for a single vortex (a) from site (1, 0); (b) from site (2, 0); (c) from site (1, 1); and (d) from site (15, 0).

The next state to notice has zero amplitude on the central site, but has a large amplitude on sites (1, 0) and (1,1). Its energy is at just less than $2t$ which puts it still within

the superconducting gap. Whereas the lowest-energy state (at the chemical potential) is similar to an s state, having a central maximum, this next state corresponds to a p-like state, and hence has a node at the centre. Labelling the states by the irreducible representations of the C_{4v} symmetry group, the central peak is an A_1 state, and the next peak a degenerate combination of E_x and E_y states. These are states like those studied by Gygi and Schluter [20] and Pöttinger and Klein [24]. Using the recursion method, the individual eigenstates cannot be studied by observing their wavefunctions, but their contributions to different Green functions can be seen. For example, the states which contribute to the current between sites i and j can be identified, by plotting the function $I_{ij}(\varepsilon)$ as defined by (7), for the same energies, ε, as the density of states on the two sites. This Green function depicts the particle contribution to the current as a function of the energy of the state. Its integral up to the chemical potential gives the current between site i and j. The function is shown in figure 2 for the links extending in the positive y direction from sites (1, 0), (2, 0), (1, 1), and (15, 0). As expected, the fully symmetric, central state does not contribute to the current. The other discrete states do give rise to currents though, with a large contribution coming from the E states.

A qualitative understanding of the contributions to the current at different energies as shown in figure 2 can be readily obtained by the following simple argument involving a uniform current carrying superconducting state, without a magnetic field. The solution of the Bogoliubov–de Gennes equation for such a one dimensional superconductor is as described by de Gennes in [21], and it will be reproduced here for the particular case of a one-dimensional lattice (i.e. a chain). A current flow in the positive x direction is described by an order parameter of the form $\Delta = |\Delta| \exp[iqx]$. Around a vortex, the current is produced by such a phase variation, but around a circle in real space instead of along a straight line. Well within a distance of the penetration depth from the centre of the vortex, the vector potential has little effect on the eigenstates, and is far from cancelling the phase variation of the order parameter. Hence it can be neglected in this qualitative discussion, as its contribution to the kinetic energy is greatly outweighed by the contribution due to the phase gradient of the wavefunctions. The two contributions are only comparable at distances where the line integral of the vector potential (and hence the flux enclosed) is of the order of the flux quantum. In other words, the paramagnetic current term dominates near the vortex centre, and only at large distances is it cancelled by the diamagnetic term. So a one-dimensional model with its variation of the order parameter can be used to give insights into states carrying a circulating current.

In order to explain the form of the current carrying function, $I_{ij}(\varepsilon)$, we shall now present an analysis of de Gennes' one-dimensional current carrying solutions. In the case with $\Delta = |\Delta| \exp[iqx]$, the current is approximately equivalent to that circulating at a distance d, where $q = 1/d$, from the vortex centre, with x on a set of discrete points along the perimeter of the circle. The eigenstates have the form

$$
\begin{aligned}
u(x) &= u_k \exp\left[i(k+q)x\right] \\
v(x) &= v_k \exp\left[i(k-q)x\right]
\end{aligned}
\tag{11}
$$

and satisfy the eigenvalue equation

$$
\begin{aligned}
\left[E_k + 2t \cos(ka + qa)\right] u_k - |\Delta| v_k &= 0 \\
-|\Delta| u_k + \left[E_k - 2t \cos(ka - qa)\right] v_k &= 0
\end{aligned}
\tag{12}
$$

where as usual, t is the hopping integral and a is the lattice spacing. The system is at half

filling, such that $\epsilon_0 + U/2 - \mu = 0$. The eigenvalues are given by

$$E_k = 2t \sin(ka) \sin(qa) \pm \sqrt{\left[-2t \cos(ka) \cos(qa)\right]^2 + |\Delta|^2} \tag{13}$$

and the corresponding eigenvectors are specified by

$$u_k^2 = \frac{|\Delta|^2}{|\Delta|^2 + \left(\left[2t \cos(ka) \cos(qa)\right] \pm \sqrt{(-2t \cos(ka) \cos(qa))^2 + |\Delta|^2}\right)^2}$$

$$v_k^2 = \frac{|\Delta|^2}{|\Delta|^2 - \left(\left[2t \cos(ka) \cos(qa)\right] \pm \sqrt{\left[-2t \cos(ka) \cos(qa)\right]^2 + |\Delta|^2}\right)^2}. \tag{14}$$

The above formulae, though quite complicated, do contain simple symmetries which explain the form of the current distributions in energy. Firstly, note that the current contribution of a state labelled by k is now proportional to $\sin(ka+qa)$ (this is the particle contribution, given by $u^*(x)u(x + a)$; the hole contribution is the same from the state of opposite energy, and opposite wavevector). Hence a state such that $k' = k + \pi/a$ has oppositely directed current to the state labelled by k. Firstly, it can be seen that there is an overall antisymmetry about the chemical potential in the current carrying states. A negative-root state, with wavevector k, has energy of opposite sign, but equal u_k and v_k amplitudes, so equal but opposite current to the state with wavevector $k' = \pi + k$ and positive energy root. So each state has a mirror state of opposite energy and current, this antisymmetry remaining in states carrying current around a vortex, as seen in figure 2. Hence, if all the states were occupied there would be no overall current flow—a result which must always hold by the orthogonality in real space of all the eigenvectors.

A second qualitative feature of the current carrying states around a single vortex is the change in sign of the current direction within a superconducting band. This feature can also be understood from the one-dimensional solutions given above. We can just consider the positive eigenvalues, which form a separate, upper band if $|\Delta| > |2t \sin qa|$. The states with wavevectors $k_1 = k$ and $k_2 = \pi - k$ have the same energy, and give rise to a current contribution at that energy of

$$I_{ij}\left(E_k^+\right) \propto \left|u_{k_1}\right|^2 \sin(ka + qa) + \left|u_{k_2}\right|^2 \sin(ka - qa) \tag{15}$$

that is

$$I_{ij}\left(E_k^+\right) = |u_k|^2 \sin(ka + qa) + |v_k|^2 \sin(ka - qa). \tag{16}$$

In the following discussion, we just consider k in the range $0 < k < \pi/2$. For $k > q$ and certainly for $k \approx \pi/2$ the above current contribution of equation (16) is clearly in the same direction as q. These states are high-energy states, near the top of the positive energy band. Within the same band, the states with wavevectors $k_3 = -k$ and $k_4 = \pi + k$ have lower energy than E_k and indeed those corresponding to $k \approx \pi/2$ which have $k_3, k_4 \approx -\pi/2$ are near the bottom of the positive energy band. They give rise to a current contribution of

$$I_{ij}\left(E_{-k}^+\right) \propto -u_{k_3}^2 \sin(ka - qa) - u_{k_4}^2 \sin(ka + qa) \tag{17}$$

that is

$$I_{ij}\left(E_k^+\right) = -u_k^2 \sin(ka - qa) - v_k^2 \sin(ka + qa) \tag{18}$$

It is seen from equation (18) that if $k > q$ then the current contribution is in the opposite direction to q and the supercurrents. Hence the direction of currents changes sign through

the positive energy band, being in the direction of the supercurrent at the top of the band and opposed to it at the bottom of the band. This is a property which is seen in the current carrying states of the single vortex.

In summary, the spectrum of single-vortex states is well described by an energy band of superconducting states carrying current around the vortex—these can be thought of as a series of racetrack states [25] of varying confined radii. There also exist discrete levels due to states localized in the vortex centre, which have a large energy spacing (and are few in number) because the coherence length, which defines the localization region, is very small. Apart from the symmetric A_1 state, the localized states also contribute to the circulating current.

3. A lattice of vortices.

In order to study the vortex lattice, a square lattice of vortices was assumed. Such a lattice should give all the qualitative features of a triangular lattice as found by Abrikosov [1], except those associated with triangular symmetry. When the underlying crystal lattice is a square lattice, it is naturally far easier to superimpose a commensurate square vortex lattice—though a triangular lattice with a much larger unit cell than the vortex cell size also can be fitted [26].

To simplify a very complicated problem, we used a square unit cell, having the same symmetry as the single-vortex solution of the previous section. Even in this case, a very complex procedure was required, to impose on the system the basic properties that a full lattice solution must possess. For example, the order parameter is zero at the central site of each unit cell, and its phase increases by 2π around each zero [27]. The phase of the order parameter cannot both be a continuous function, and be periodic, if it is to have the above property [28]. The only way to maintain its periodicity is to treat each unit cell in a different gauge. The complete system was solved in a particular gauge chosen according to the requirement that the configuration of charges, order parameters, and vector potentials, $\{n_i, \Delta_i, A_{ij}\}$, in one unit cell had the most symmetric form. From this configuration, all the other configurations in the other unit cells are calculated, by carrying out an appropriate gauge transformation. The procedures of the recursion method were carried out using a Hamiltonian which is not invariant upon translations between vortex cells, but which is given through all space in one specific gauge. Self-consistent calculations were made as usual, but so as to give the set of quantities $\{n_i, \Delta_i, I_{ij}, \Phi_n, A_{ij}\}$ in the first unit cell only. The corresponding quantities in other unit cells are obtained by the transformations given below. The indices α and β label the unit cell number, in vortex lattice spacings, from the central cell. The indices i and j label the coordinates of a lattice site within a unit cell, such that the central site is labelled by $(i, j) = (0, 0)$.

$$
\begin{aligned}
n_{ij}^{\alpha\beta} &= n_{ij}^{00} \\
\Delta_{ij}^{\alpha\beta} &= \Delta_{ij}^{00} \exp\left[2i\chi_{ij}^{\alpha\beta}\right] \\
I_{ij,kl}^{\alpha\beta} &= I_{ij,kl}^{00} \\
A_{ij,kl}^{\alpha\beta} &= A_{ij,kl}^{00} + \left(\frac{\hbar}{e}\right)\chi_{kl}^{\alpha\beta} - \left(\frac{\hbar}{e}\right)\chi_{ij}^{\alpha\beta}.
\end{aligned}
\tag{19}
$$

The vector potential above is defined along the link $(i, j) \mapsto (k, l)$ so that

$$
A_{ij,kl}^{\alpha\beta} = \int_{r_{kl}}^{r_{ij}} A(r') \cdot dr'.
\tag{20}
$$

The choice of gauges is such that both the phase of the order parameter and the vector potential are single valued along the boundaries of unit cells, with a symmetric gauge form of the order parameter's phase in the central cell. Such a criterion leads to the choice

$$2\chi_{ij}^{\alpha\beta} = \frac{\alpha\pi j}{n} - \frac{\beta\pi i}{n} + (\alpha + 1)(\beta + 1)\pi + \pi \tag{21}$$

where the unit cell has size $na \times na$ so contains $n \times n$ sites. The phase of the order parameter, Δ, and the corresponding gauge parameter, χ, are depicted in figures 3 and 4 for the four unit cells $(\alpha, \beta) = (0, 0), (1, 0), (0, 1)$, and $(1, 1)$. Note that Bloch's theorem can be used with a supercell of 2×2 vortex cells using the above gauge function, corresponding to that of Canel [29] provided the phases there are corrected with the missing factor of $\frac{1}{2}$.
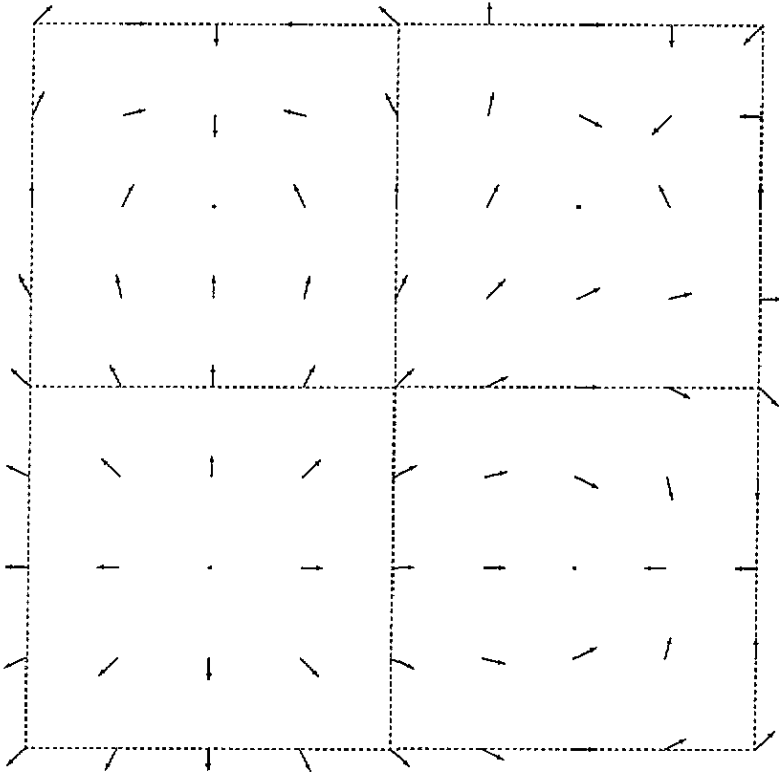
Figure 3. The phase variation of the order parameter as a continuous function, shown schematically through four vortex cells.

With such a scheme in place, self-consistent solutions were found in the same manner as for a single vortex. A number of different-sized unit cells were used, corresponding to different average magnetic fields through the sample. The cells were all square, with the vortex centre on the central site, so each cell contained $N = 2n \times 2n$ plaquettes, where n is an integer. Solutions were found for all n up to $n = 15$, which corresponds to a magnetic field given by $Ba^2 = h/2Ne$ where $N = 900$ (and the flux per plaquette is $p/q = 1/1800$ in units of the electronic flux quantum, h/e, which figures in the normal state, namely the Hofstadter, problem [30]). The calculations were carried out at half filling, giving $n = 1$ on every site, and for a large interaction energy of $U = -6t$ for the same reasons as given for the single-vortex calculations. Usually the recursion method was
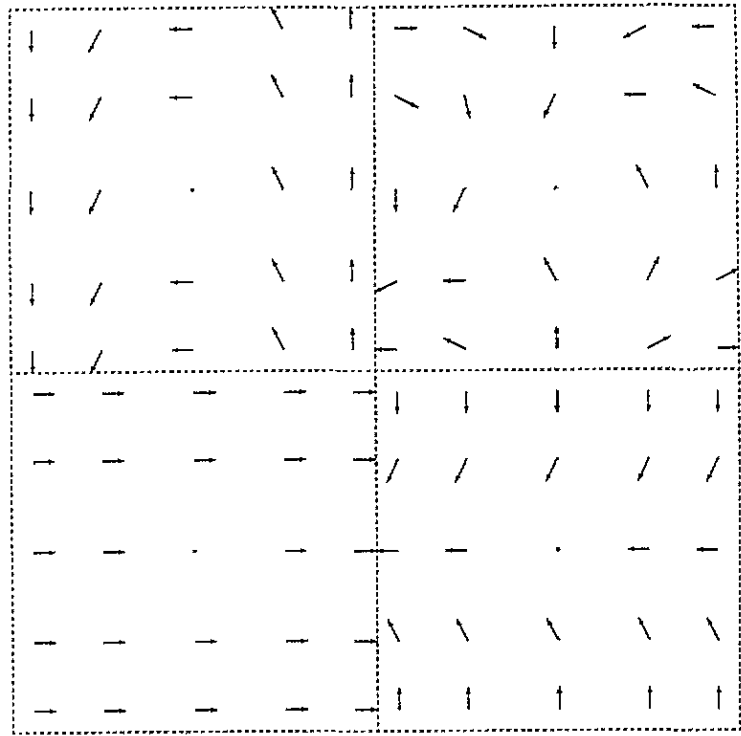
Figure 4. The corresponding values of the gauge parameter, given as an angle: $\exp[2i\chi]$.

carried out on each site to give thirty coefficients exactly, and this was extrapolated up to more than 1000. The extrapolation was not generally a good fit, as the coefficients were not following any obvious pattern. This means that fine detail in the spectrum should not be taken at face value, although integrals over the weight of the density of states is still given to excellent accuracy. Consequently, integrated quantities like n_i, Δ_i, and I_{ij} were accurately determined, as evidenced by the cancellation of the currents to any particular site.

The form of the self-consistent solution for a magnetic field corresponding to $Ba^2 = \frac{1}{128}(h/e)$, that is a vortex cell containing 8×8 plaquettes, is given in figures 5–7. The phase variation of the order parameter is as depicted in figure 3, increasing by 2π around each vortex centre, while its magnitude, figure 5, is seen to plummet to zero at these points. The short coherence length, resulting from the overly large value of the order parameter (and interaction energy), is small enough to allow the normal state hole to be almost fully healed within one lattice spacing. The order parameter is then approximately constant in magnitude between vortices. A point in the results, which cannot be seen from the picture, is that the maximum in the magnitude of the order parameter occurs a few sites from the vortex centre, and in the diagonal (1, 1) direction. This maximum is shallow, but naively one would have expected it to be at the furthest point from the vortex centres. This is thought to be an artifact of the extremely short coherence length here [15].

The current distribution for one such unit cell is shown in figure 6. The arrows, whose lengths are proportional to the current along each particular link, depict a circulating flow around the vortex centre, as expected, with no flow along the radial (1, 0) directions. The currents are at a maximum nearest the vortex centre, due to the short coherence length, and
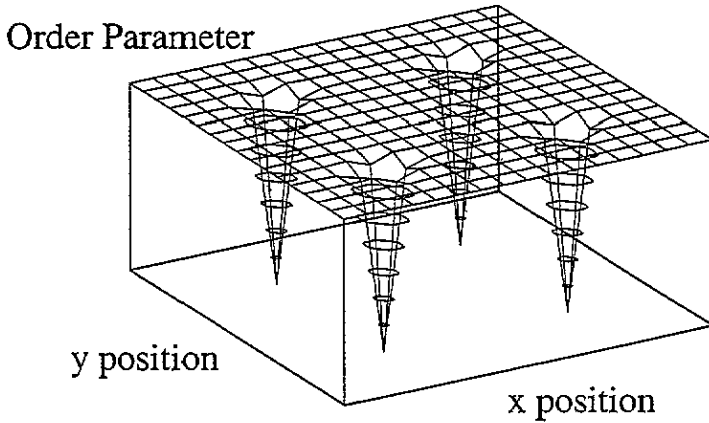
Magnitude of order parameter for 8x8 vortex cells

Figure 5. Magnitude of the order parameter on sites of four vortex cells with 8 × 8 unit cell.
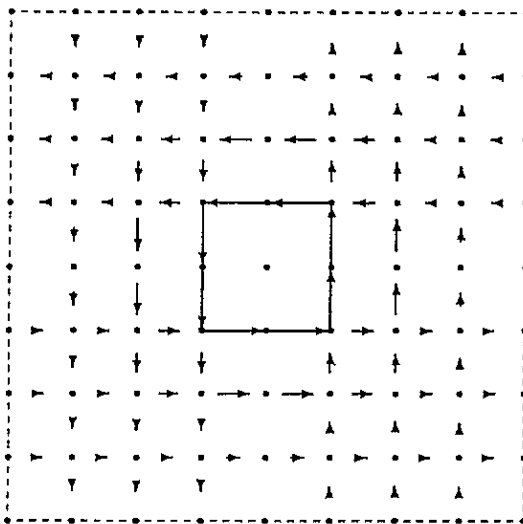

Figure 6. The current distribution for an 8 × 8 vortex cell.

are zero along the unit cell boundaries, as is necessary by symmetry. In fact, it is the latter point which determines the total flux within the unit cell to be the superconducting flux quantum, $h/2e$. It is the current distribution which maintains the magnetic field variation shown in figure 7 for four such vortex cells. So the magnetic field is changing most near the vortex centres, and is more constant where the current is small. Naturally the maximum field is at the vortex centre, but note the overall field change is of the order of one per cent, as the penetration depth ($\lambda = 100a$) is much greater than the vortex spacing ($8a$).

Further information can be obtained from the density of states. We shall investigate both the density of states local to an individual site, and the total density of states. The latter is the sum of the former over all sites in a vortex cell. Unfortunately, interesting features of the magnetic field structure would not be observable for large unit cells where

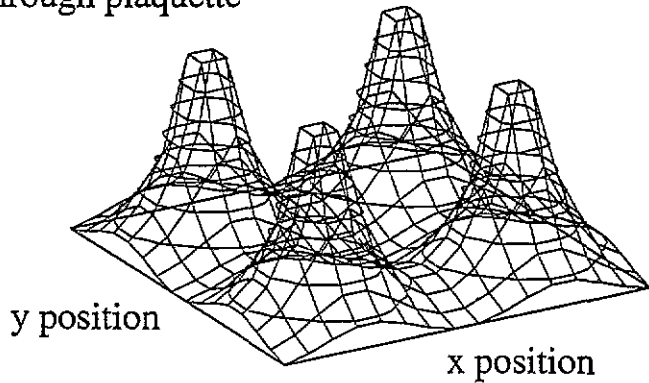Magnetic field variation for 8x8 vortex cells

Flux through plaquette

Figure 7. The magnetic field through plaquettes of four vortex cells with 8×8 unit cell. Note the absolute variation is only of the order of one per cent—the zero is off the graph.

the field is low. This is because the Landau level spacing would be less than the detail given in the density of states by the recursion method. An understanding of this problem is gained by realizing that for the full details of orbits to be seen in the spectrum, accurate coefficients must be found in the recursion method, for Lanczos states which extend over the whole of the Landau orbits. The criterion in the normal state is that for a magnetic field with p/q electronic flux quanta (h/e) per plaquette, the recursion coefficients, a_n and b_n, must be calculated out accurately up to $n > q$. This is because all q Landau-like levels within the band will correspond to orbits containing up to q electronic flux quanta, and hence with area $q \times q$. Thus to stand a chance of observing the effects of any quantization of the levels in the superconducting state, a large field and small vortex cell must be used. Consequently, in what follows, the densities of states are given for a self-consistent solution of a 4×4 unit cell. In this case there is one superconducting flux quantum $(h/2e)$ per sixteen plaquettes, and for the electronic flux quantum (h/e), the magnetic cell contains 32 plaquettes, so $p/q = 1/32$. In figure 8(a) we display the local density of states for the centre of a vortex, that is site $(0, 0)$. As in the case of a single vortex discussed in the previous section, the large peak at the chemical potential corresponds to an essentially localized s state at the vortex centre. Of course, for the infinite array of vortices with which we are concerned here, such localized states form a band. However, we find a negligible bandwidth, and the amplitude of the state is exponentially reduced on moving away from the vortex centre. Figures 8(b), (c) and (d) show the local densities of states on sites $(1, 0)$, $(2, 0)$, and $(1, 1)$ respectively. Note the sites neighbouring the vortex centre reveal angular momentum states like those of the single vortex. Further from the vortex centre, there is a clear discretization of the superconducting band, which is also revealed in the total density of states, figure 9(a). For comparison, the density of states for a normal band in the same magnetic field is given in figure 9(b).

Following on from our study of the current carried by links around the single vortex, plots of the same functions, $I_{ij}(\varepsilon)$, for the flux lattice, for the y currents from sites $(1, 0)$ and $(1, 1)$, are given in figure 10. The states are of course discrete now, due to the strong magnetic field, but the overlying envelope function is very similar to that for the single
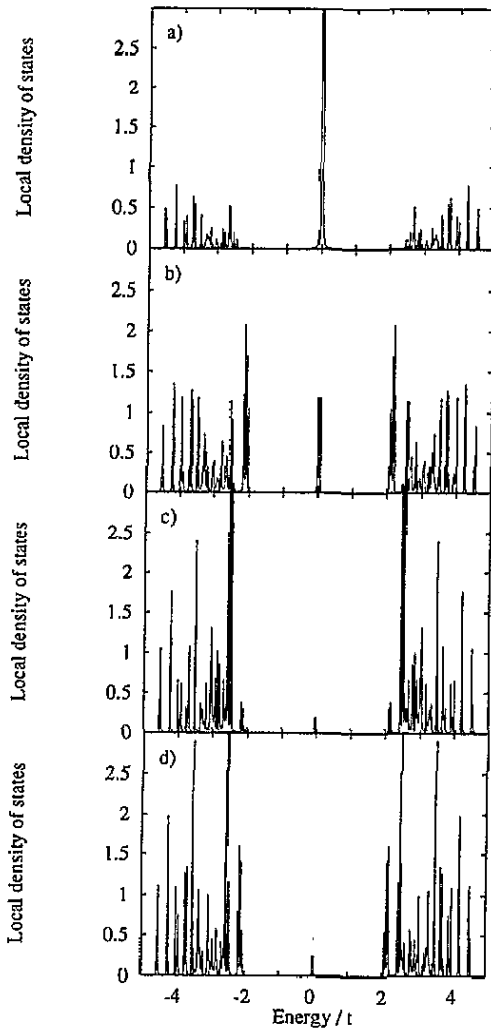
Figure 8. Local densities of states for various sites of a vortex lattice, with 4 × 4 unit cell (a) on site (0, 0); (b) site (1, 0); (c) site (2, 0); and (d) site (1, 1).

vortex. Hence the principal effect of the magnetic field is to break up the spectrum into sharp peaks. At least near the vortex centre, where the phase gradient of the order parameter dominates the vector potential, other effects on the states appear less significant.

In short, the most striking feature of the above density of states curves, and the central result of this paper, is that in both the normal and superconducting state, the effect of a magnetic field on a spectrum is to split continuous bands into discrete Landau-like peaks. This is already known to occur within the normal regions of a type II superconductor [24], but here we find it just as pronounced in the superconducting regions where the order parameter has constant magnitude and is large. The separation of levels is inversely dependent on the zero-field density of states at that energy, so many discrete levels are squashed into the singularities at the edges of the gap in a superconductor, in a similar way to those at the van Hove singularity at the centre of the two-dimensional band (figure 9(b)). Of course, in the vortex state, the situation is more complex, because the magnetic field has
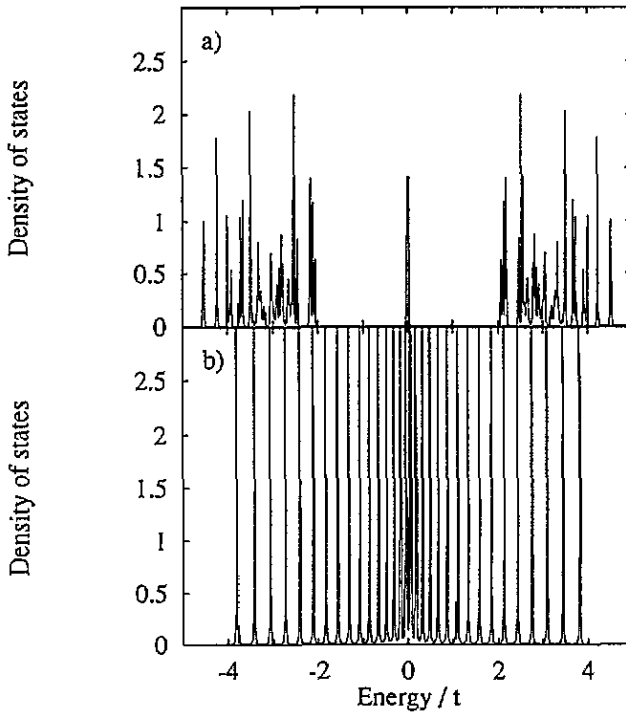
Figure 9. (a) The density of states for a vortex lattice, with 4×4 unit cell, hence $Ba^2 = (1/16) (h/2e)$, and (b) the normal state density of states in the same magnetic field.

changed the structure of the potentials which broadens the peaks in the density of states. Thus, it may be said that the superconducting ground state is formed from Cooper pairs whose members individually occupy discrete Landau levels. Note that whilst many theories start solving the Bogoliubov–de Gennes equation by expanding the solution in terms of Landau orbitals [2, 3, 4, 5, 6], we did not do so here. Thus our results can be taken as convincing evidence that, at least in the parameter range studied, the Landau levels play the above role. Clearly, this suggests that the superconducting ground state energy should oscillate with magnetic field variation [2, 3] as in the normal state. Therefore we conclude that normal electrons may not be necessary for the de Haas–van Alphen effect. In the following section we shall show that this is indeed the case.

4. Oscillations of the thermodynamic potential

To study the possibility of de Haas–van Alphen oscillations in the superconducting state in a similar vein to the work of Lifshitz and Kosevich in the normal state [31], we use the form of the generalized thermodynamic potential [11]

$$
\Omega^{SC} = -\frac{1}{2\beta} \sum_\lambda \left[\log \left\{ 1 + \exp \left[-\beta \left(\varepsilon_\lambda^{(\mu)} \right) \right] \right\} - \log \left\{ 1 + \exp \left[\beta \left(\varepsilon_\lambda^{(\mu)} \right) \right] \right\} \right.
$$

$$
\left. + \log \left\{ 1 + \exp \left[-\beta \left(E_\lambda \right) \right] \right\} + \log \left\{ 1 + \exp \left[\beta \left(E_\lambda \right) \right] \right\} \right]
$$

$$
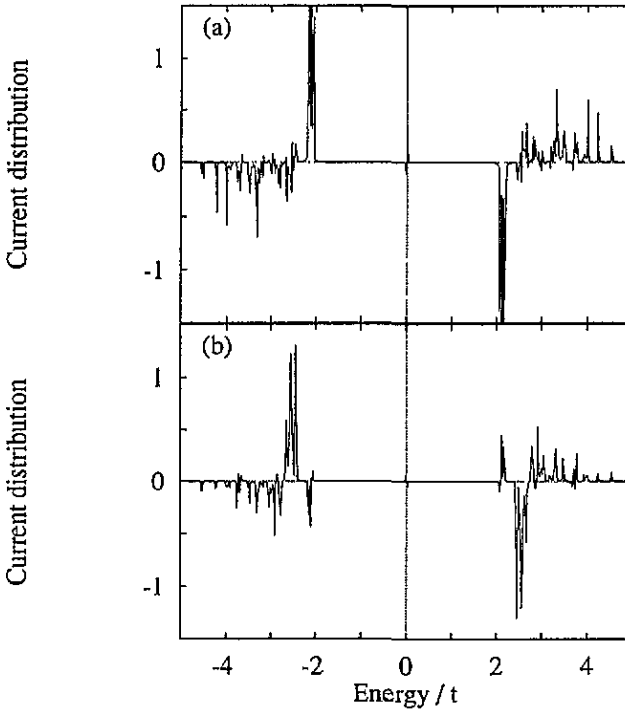- \sum_i \frac{|\Delta_i|^2}{U} - \sum_i \frac{U n_i^2}{4}. \tag{22}
$$

Figure 10. y current distribution in energy for links of the flux lattice with a 4×4 unit cell: (a) from site $(1, 0)$ to $(1, 1)$ and (b) from site $(1, 1)$ to $(1, 2)$.

In the above expression, $\varepsilon_\lambda^{(\mu)}$ is the quasiparticle energy of the normal state, measured from the chemical potential, and $\partial \varepsilon_\lambda^{(\mu)} / \partial \mu = -1$ for all λ. E_λ is the positive quasiparticle energy eigenvalue of the Bogoliubov–de Gennes equations. To lay the foundation of further discussion, we now substantiate the above expression for Ω^{SC}.

Explicit differentiation of the above grand potential leads to

$$\overline{N} \equiv -\frac{\partial \Omega^{SC}}{\partial \mu} = \sum_\lambda \frac{1}{2} - \frac{1}{2} \left(\frac{\partial E_\lambda}{\partial \mu} \right) \left[f(E_\lambda) - f(-E_\lambda) \right] \tag{23}$$

using the identity

$$\left(\frac{\partial E_\lambda}{\partial \mu} \right) = -\sum_i \left(|u_i^\lambda|^2 - |v_i^\lambda|^2 \right) \tag{24}$$

proved in appendix B; this yields the conventional formula for the total number of electrons, $\overline{N}$.

Similarly, differentiation with respect to the order parameter leads to

$$\frac{\partial \Omega^{SC}}{\partial \Delta_i} = \sum_\lambda \left(\frac{\partial E_\lambda}{\partial \Delta_i} \right) \left[1 - 2f(E_\lambda) \right] - \frac{\Delta_i^*}{U}. \tag{25}$$

Requiring that the equilibrium values, $\{\Delta_i\}$, minimize the grand potential in equation (22), and therefore setting the right-hand side of equation (25) to zero, leads to the correct gap equation for the order parameters, $\{\Delta_i\}$, provided

$$\left(\frac{\partial E_\lambda}{\partial \Delta_i} \right) = \left(u_\lambda^i \right)^* v_\lambda^i \tag{26}$$

as shown in appendix B. Note that as $\partial\Omega^{SC}/\partial\Delta_i = 0$, to first order oscillations in the order parameter do not explicitly affect the thermodynamic potential. The above differential relations, and the fact that the normal state thermodynamic potential must be reached in the limit $\Delta \mapsto 0$, verify the form of equation (22) for the grand potential in the superconducting state. As will be evident presently, it is a very useful starting point for discussing the dependence of Ω^{SC} on the external magnetic field, B.

With the above preliminaries, let us now work out the diamagnetic moment of a metal. For the normal state we find

$$M^N = -\frac{\partial\Omega^N}{\partial B} = -\frac{\Omega^N}{B} + \sum_\lambda \frac{\partial\varepsilon_\lambda}{\partial B} f(\varepsilon_\lambda) \qquad (27)$$

while for the superconducting state

$$M^{SC} = -\frac{\partial\Omega^{SC}}{\partial B} = -\frac{\Omega^{SC}}{B} + \sum_\lambda |u^\lambda|^2 \frac{\partial\varepsilon_\lambda}{\partial B}\bigg|_\Delta f(E_\lambda). \qquad (28)$$

A full calculation shows that in the above two equations (27) and (28) the contribution to the oscillatory part of the magnetization is of order $\varepsilon_F/\hbar\omega_c$ $(= n_F \gg 1)$ greater for the second terms than the first. Hence, to lowest order in $1/n_F$, the first terms, of the form Ω/B, can be neglected in a discussion of contributions to the de Haas–van Alphen effect. Consequently, the dominant effect of superconductivity on the oscillatory magnetization is seen to be due to the appearance of the particle probability amplitude, $|u^\lambda|^2$, in the second term of equation (28). This results in the energy cut-off for electron occupation of levels being broadened not only by the Fermi function, $f(E_\lambda)$, on the scale of kT, as in the normal state, but also by $|u^\lambda|^2$, which falls from unity to zero over an energy range of order Δ.

This effect is illustrated in figure 11 which provides a simple view of the process. As the magnetic field is increased, the effect of the increase in gradient of the lines of ε_n against n can be viewed as a spreading of the discrete states from left to right as their energy separation increases. In the normal state, filled electron states which contribute to the total energy, after increasing in energy, become emptied as they pop up through the chemical potential (which does not vary much for 3D materials, and indeed is constant for a half-filled band in the 2D case that we studied in section 3). So the well known result is that the total energy and hence magnetization oscillates at the frequency with which the electron states cross the chemical potential. The hole states mirrored in the chemical potential can be ignored in the normal state.

In the superconducting state, there are two differences. Firstly, the dispersion curve need not cross the chemical potential due to the superconducting gap. Secondly, particle-like states are depleted of electrons (and hence reduce their contribution to the total energy) over a region of order $|\Delta|$ before they reach the gap. The electrons move into the corresponding hole-like state (with $|v|^2 > |u|^2$) in this region and the particle–hole coupling means that these states cannot be ignored in superconductors. It is not until a particle-like state is at an energy of order $|\Delta|$ above the gap that its corresponding hole-like state is effectively emptied of electrons, so its contribution to the total energy is negligible. This very gradual emptying of electrons from a state over an energy range of the order of $|\Delta|$ (rather than an abrupt depletion on crossing the Fermi surface) reduces the amplitude of the oscillations, just as a temperature does by broadening the Fermi–Dirac occupation function at the chemical potential. In fact, the functional forms of the two independent damping factors are seen to be somewhat similar.
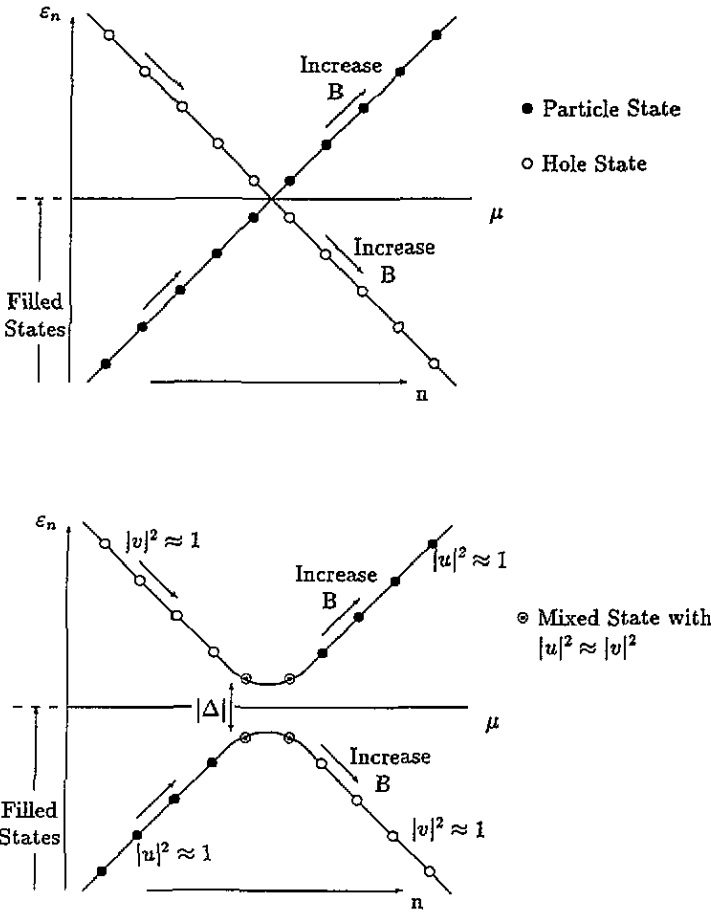
Figure 11. Particle-like states move up in energy with increasing field, while hole-like states move down in energy. Only particle amplitudes contribute to the thermodynamic potential.

Having established the form of the grand potential in the superconducting state, we can use the simplified semiclassical approximation

$$E_{n,\sigma} = \sqrt{\left(\varepsilon_{n,\sigma}^{(\mu)}\right)^2 + |\Delta|^2} \tag{29}$$

where $\varepsilon_{n,\sigma}^{(\mu)} = \varepsilon_n + \epsilon_\sigma - \mu$. Such a form is suggested by the observation of the density of states for the vortex lattice of the previous section 3 (neglecting the normal region states) and it also follows from an approximate semiclassical theory [32] given in appendix 6.

Using equation (29), the method of Lifshitz and Kosevich [31] can be followed in evaluating equation (22) for Ω^{SC}. The result contains those terms found in the usual normal state problem, unless indicated. The combination of the first two terms in the thermodynamic potential (equation (22)) gives no oscillatory contribution, while the next two terms yield

$$\Omega_l^{(osc)} = \frac{V(eB)^{5/2}}{2^{3/2}\pi^{7/2}\hbar^{1/2}m^*l^{5/2}} \left| \frac{\partial^2 A(\mu, k_z)}{\partial k_z^2} \right|_{ex}^{-1/2} \cos\left(2\pi\epsilon_{\sigma+}/\hbar\omega_c\right)$$

$$\times \mathrm{Re} \left\{ \frac{2\pi\mathrm{i}\, l m^*}{\hbar e B} \int_{-\infty}^{\infty} \frac{\varepsilon_\sigma^{(\mu)} \exp\left[2\pi\mathrm{i}\, l\, (\partial n/\partial\varepsilon)_{\varepsilon_\sigma^{(\mu)}=0}\, \varepsilon\right] \mathrm{d}\varepsilon}{\sqrt{\varepsilon_\sigma^{(\mu)2} + \Delta^2}} \right.$$

$$\left. \times \left[1 - 2f(\sqrt{\varepsilon_\sigma^{(\mu)2} + \Delta^2})\right] \right\} \tag{30}$$

for the oscillatory contributions to the thermodynamic potential. Upon differentiating the above expression with respect to B, it contributes to the magnetization as

$$M_z^{(osc)} = \sum_{ex} \sum_{l=1}^{\infty} (-1)^{l+1} \frac{\hbar A^{(ex)}(\mu)}{eB} \Omega_l \sin\left[\frac{\hbar A^{(ex)}(\mu)}{eB} \pm \frac{\pi}{4}\right] \tag{31}$$

which has the same form as in the normal state. In particular, $A^{(ex)}(\mu)$ is the area of the extremal orbit of the quasiparticle around the normal state Fermi surface, perpendicular to the magnetic field. Clearly the frequency of oscillation is unchanged by superconductivity. On the other hand, the damping factors within Ω_l, due to the terms in curly brackets of equation (30), are now quite different from the corresponding factors in the normal state [33]. In the latter case, the damping term in Ω_l is given by $\lambda/\sinh(\lambda)$, where $\lambda = 2\pi^2 l k T m^*/\hbar e B$, and is due to the thermal broadening of the distribution function, $f(\varepsilon)$. For the superconducting state we find a simple analytic solution only in the limit where $\Delta \gg kT$. In this case, the Fermi factor can be treated as unity for states below the gap and zero for those above the gap. This leads to a damping factor in Ω_l of $aK_1(a)$, where the coefficient a is $2\pi l$ times the gap parameter, Δ, divided by the normal state Landau level spacing at the chemical potential, $\hbar\omega_c$; namely $a = 2\pi l \Delta/\hbar\omega_c$. From the asymptotic form of the Bessel function of imaginary argument at large a it follows that

$$K_1(a) \approx \sqrt{\frac{\pi}{2a}} e^{-a} \qquad \text{for } a \mapsto \infty \tag{32}$$

where it is seen that when the order parameter exceeds the Landau level spacing, an exponential damping term is introduced. The factor $aK_1(a)$ approaches unity as $1 - a^2$ as the order parameter approaches zero, and the normal state is reached in a manner consistent with $e^{-c\Delta^2}$ (where c is a constant) as suggested by Maki [34]. The function $aK_1(a)$ is plotted in figure 14 to give an indication of its effect.

Note that the above results show that de Haas–van Alphen oscillations can exist when normal regions of a sample are neglected, and the whole Fermi surface is gapped in the superconducting state—even at zero temperature. The oscillations come from oscillations in the superconducting ground state energy. Of course, the above results have been derived by using only an approximate treatment of the semiclassical theory in appendix C, and the scattering due to phase variation of the order parameter is not *explicitly* taken into account. Note however, that the phase variation is included implicitly since neglecting $\nabla\Sigma - eA$ prevents large current terms influencing the spectrum. Clearly, the current proportional to $\nabla\Sigma - eA$ would increase with $A(r)$ at large r unless the phase of the order parameter varies so as to maintain a finite current.

5. Simple computational results

To lend further credence to the above analytic results, we have performed a number of approximate numerical calculations of the free energy in a magnetic field. First we studied a two-dimensional square lattice Hubbard model in the normal state. This is effectively the
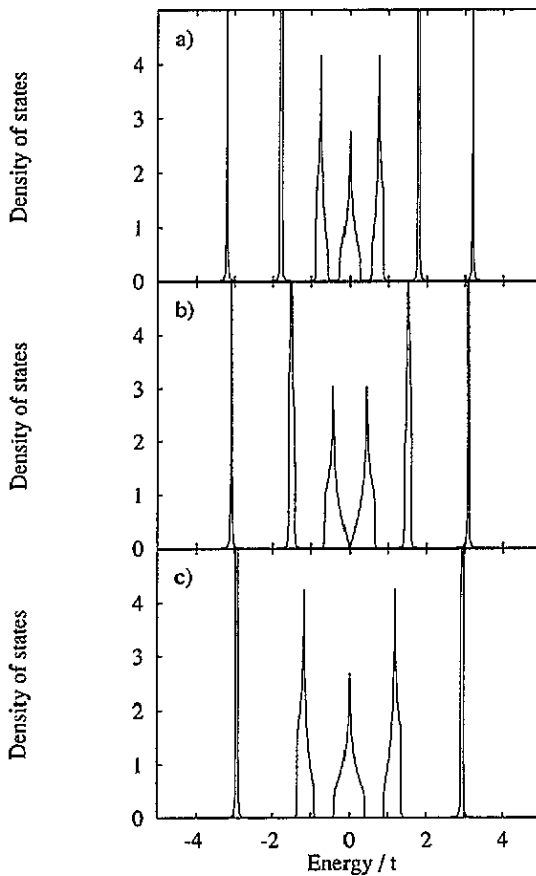
Figure 12. The normal state density of states for magnetic fields of a) $p/q = \frac{1}{7}$; b) $p/q = \frac{1}{6}$; and c) $p/q = \frac{1}{5}$ where p/q is the magnetic flux per plaquette, Ba^2, in units of the electronic flux quantum, h/e.

same system whose spectrum of allowed energy states as a function of magnetic field per plaquette was made famous by Hofstadter [30]. The calculations are carried out using the recursion method, and for a half-filled band. The total energy was calculated as the sum, up to the zero of energy, over all the Hofstadter states at a given field. The densities of states for fields corresponding to $\frac{1}{7}$, $\frac{1}{6}$, and $\frac{1}{5}$ of a flux quantum per plaquette are shown here in figures 12(a)–(c) as calculated by recursion. If the chemical potential is at the zero of energy, the situation as the field increases is a little different from that for free electrons. With free electrons, the Landau levels all increase in energy with field, and their spacing increases uniformly with field, so levels move up through the chemical potential as the field is changed. In the Hofstadter spectrum, this is true for the lowest energy levels, where the zero-field band is approximately parabolic. However, the states at the top of the band also have an approximately parabolic dispersion in the normal state, but with opposite curvature, so have negative effective mass and come down in energy with increasing magnetic field. The overall effect that is seen in the Hofstadter spectrum as the field is increased is that levels near the edge of the spectrum move towards the centre, where they collide and cancel each other. The degeneracy of the remaining levels increases to keep the total number of states constant. This effect can be seen in figures 12(a)–(c) as the field increases from

$p/q = \frac{1}{7}$ to $\frac{1}{6}$ to $\frac{1}{5}$. In between these simple, rational fields, the spectrum follows a richly structured evolution as the field changes, with splitting and reorganization of bands. This can be seen from the full spectrum. Nevertheless, this complicated behaviour leads to a smooth variation of the total energy. From the densities of states shown, it is apparent that for simple rational fields, p/q, with $p = 1$, the total energy at half-filling is a minimum for q an even integer, and a maximum for q odd, when occupied states are closest to the chemical potential (a constant at zero energy). This is what is seen in the variation of total energy with magnetic field, as shown in figure 13. The oscillations for Hofstadter levels are naturally in $1/B$, just as they would be for Landau levels of elementary discussions [35]. We get well defined oscillations because, thanks to the recursion method, we are able to calculate Ω for arbitrary fields. Obviously, this is due to the fact that, for this real space method, there is no requirement for a supercell to exist commensurate with the lattice spacing.

The effect of superconductivity on these oscillations can be seen in a very simple manner. Without carrying out a fully self-consistent calculation to find the vortex lattice, an off-diagonal particle–hole coupling term (or pairing potential), corresponding to a constant order parameter, can be introduced into the Hamiltonian. The recursion method as formulated for superconductivity [15] can then be carried out and the total energy calculated as a function of magnetic field, for different values of the pairing potential, Δ. Computationally the method is rapid, as each site is physically the same so recursion need only be carried out from one site to find the density of states.

The results are shown in figure 13 over a small field range, and for a number of values of the off-diagonal pairing potential. The coupling, if small, has little effect on the oscillations, but eventually damps them out, as expected. The finite-temperature method of Nicholson and Stocks [16] was used to calculate the energy, at a temperature such that $kT = 0.01t$. In the units given, the continuum limit Landau level spacing, $\hbar\omega_c = \hbar eB/m^*$, is equal to $4\pi tp/q$ where the continuum effective mass of $m^* = \hbar^2/2ta^2$ has been used [32]. This means, for example, that when the magnetic field has $p/q = 0.01$, a pairing potential of $\Delta \approx 0.12t$ would correspond to a typical Landau level spacing. It is however a little difficult to be precise where the spacing of Hofstadter levels is concerned, as it is apparent from the spectrum that the level spacing is far from constant, and indeed approaches zero (corresponding to an infinite effective mass) at its centre.

However, an attempt can be made to compare these results to the analytic ones of the previous section for the magnitude of damping by the order parameter. At two different fields ($p/q = \frac{1}{18}$ and $p/q = \frac{1}{22}$) the magnitude of the oscillation, as a fraction of that in the normal state, is plotted against the pairing potential, in the form $2\pi\Delta/\hbar\omega_c = \Delta q/2tp$, in figure 14. The thermal damping in the normal state gives values for $\lambda/\sinh\lambda$ (where $\lambda = 2\pi^2 kT/\hbar\omega_c$) of 0.99 and 0.98 respectively, so has little effect—and for most of the graph, $\Delta \gg kT = 0.01t$. The analytic damping factor of the previous section is given by the continuous line, and only very roughly gives the reduction in amplitude as seen in the computational data. In general, the computational data give less damping, which might be due to the form of constant Δ used in the recursion method, which does not give rise to a gap in the spectrum as large as $|\Delta|$. However, the point is made, once again, that the presence of a gap, with the loss of Fermi surface, does not completely destroy de Haas–van Alphen oscillations, but merely introduces a damping term.

6. Conclusions

A Bogoliubov–de Gennes equation of tight-binding form was solved self-consistently with Ampère's law on the lattice using a real space recursion method. It was designed to describe
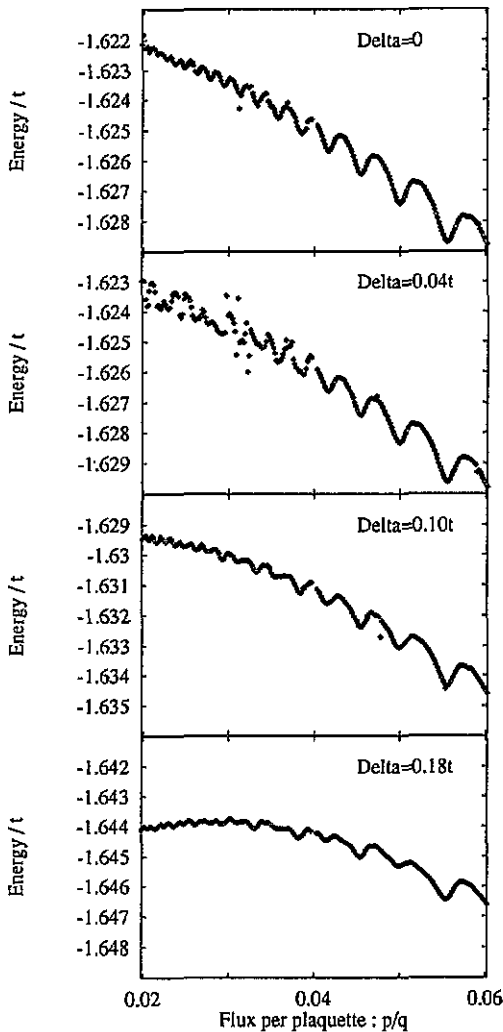
Figure 13. Effect of a pair potential, $\Delta = 0.04t$, $0.10t$ and $0.18t$ on the normal de Haas–van Alphen oscillations (top), evaluated by the recursion method.

the quasiparticle spectrum of an Abrikosov flux lattice corresponding to the ground state of a type II superconductor in a magnetic field. The structure of the ground state was found to be that of filled Landau-like states. Based on these and other, approximate, calculations, it was argued that the grand potential is an oscillatory function of $1/B$, where B is the magnetic field in the sample, with the same frequency as in the normal state without any explicitly normal region being present. Furthermore, it was shown that these de Haas–van Alphen oscillations are damped by the presence of a gap according to the formula given in equation (30).

Unfortunately, if we choose the gap, $\overline{\Delta}$, in the simple analytic model for the spectrum to be the thermodynamic averaged gap $(\overline{\Delta}(B) \approx \overline{\Delta}(0)\sqrt{1 - B/B_{c2}})$ the damping by superconductivity as predicted by the above interpretation of the numerical solutions is too high—the experimentally observed damping of the oscillation amplitude corresponds to a gap of approximately one third of the thermodynamic value. Thus further investigation
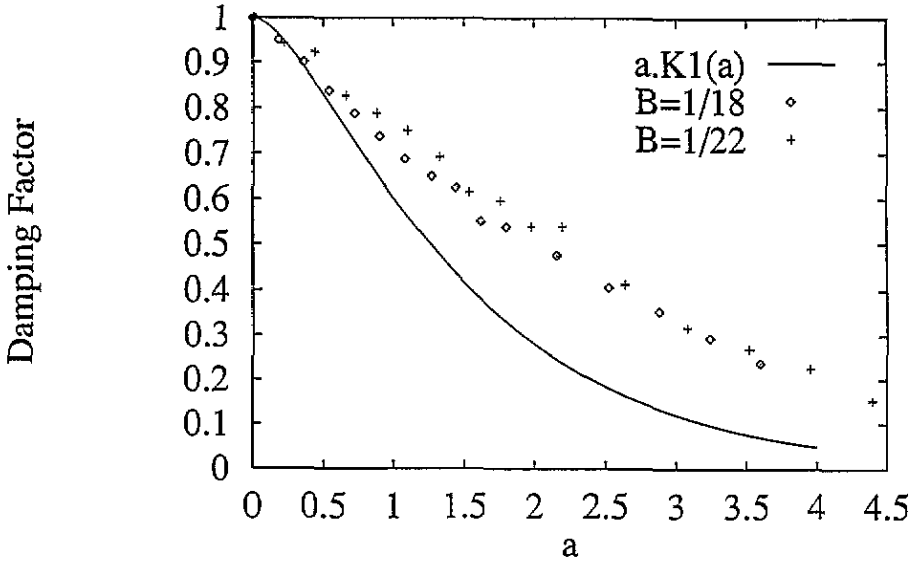
Figure 14. Comparison of the analytic and numerical results for the damping of de Haas–van Alphen oscillations against superconducting gap parameter, Δ.

of the precise meaning of the effective gap, $\overline{\Delta}_{eff}$, is required.

In conclusion, we wish to stress that the real space approach afforded by the recursion method proved extremely efficient in describing Landau-like levels, particularly because the technique is ideally suited to numerical parallelization.

Acknowledgments

Appendix A. Maxwell's equations on a lattice

In order to find the magnetic field due to induced currents, one must solve the relevant Maxwell's equations for the vector potential. These are

$$\nabla \times \nabla \times A(r) = \mu_0 j_{ind}(r) = \mu_0 \nabla \times M(r) \tag{A1}$$

where $j_{ind}(r)$ is the induced current density, which can be described as the curl of the magnetization density, $M(r)$ and μ_0 is the permeability of free space.

In a discretized version of the above equation, the set of link currents between sites is described by a set of loop currents around plaquettes, each of which gives rise to a magnetic moment in the direction normal to the current loop. The induced magnetization within a plaquette is proportional only to the circulating current loop around it. This can be shown by the following argument, based on an explicit differentiation of the Hamiltonian with respect to the magnetic field to give the magnetization operator, in the Poincaré gauge [36].

For a time-invariant magnetic field, $B(r)$, in the Poincaré gauge, the vector potential, $A(r)$, is given by [37]

$$A(r) = \int_0^1 [B(\lambda r) \times r] \lambda \, d\lambda. \tag{A2}$$

Clearly, this relation is equivalent to the one which defines the symmetric gauge in the special case of a magnetic field which is constant throughout space ($A^{sym}(r) = (B/2)(-y, x, 0)$).

Now the operator for the magnetization per unit volume at a point in space, r, is given by the functional derivative of the Hamiltonian with respect to the magnetic field at that point, $B(r)$ [31]. The magnetic field only occurs in the phase of the hopping integral, so the differential of the Hubbard Hamiltonian with respect to magnetic field only contributes through kinetic energy terms in the form

$$\frac{\delta \hat{H}_{ij}}{\delta B(r)} = \sum_\sigma \hat{c}_{i\sigma}^\dagger \hat{c}_{j\sigma} \frac{\delta t_{ij}}{\delta B(r)} + \hat{c}_{j\sigma}^\dagger \hat{c}_{i\sigma} \frac{\delta t_{ji}}{\delta B(r)} \tag{A3}$$

which is

$$\frac{\delta \hat{H}_{ij}}{\delta B(r)} = \sum_\sigma \hat{c}_{i\sigma}^\dagger \hat{c}_{j\sigma} \frac{\delta}{\delta B(r)} \left(-t \exp\left[-\frac{ie}{\hbar} \int_{r_i}^{r_j} A(r') \cdot dr'\right]\right) - \text{HC} \tag{A4}$$

or

$$\frac{\delta \hat{H}_{ij}}{\delta B(r)} = \hat{c}_{i\sigma}^\dagger \hat{c}_{j\sigma} \frac{ite}{\hbar} e^{\pm A_{ij}} \frac{\delta}{\delta B(r)} \left(\int_0^1 \lambda \, d\lambda \int_{r_i}^{r_j} [B(\lambda r') \times r'] \cdot dr'\right) - \text{HC} \tag{A5}$$

where

$$A_{ij} = (ie/\hbar) \int_{r_i}^{r_j} A(r') \cdot dr'$$

and where $\hat{c}_{i\sigma}^\dagger$ and $\hat{c}_{i\sigma}$ are creation and annihilation operators for an electron of spin σ on site i, and HC indicates the Hermitian conjugate of the previous term. A link, $r_i \mapsto r_j$, only gives a contribution if it crosses a line drawn from the origin through the point r to infinity after it has extended beyond the point r, in this case there is a point, r', on the link such that $\lambda r' = r$, for $0 \leqslant \lambda \leqslant 1$. Such links are shown in figure A1.
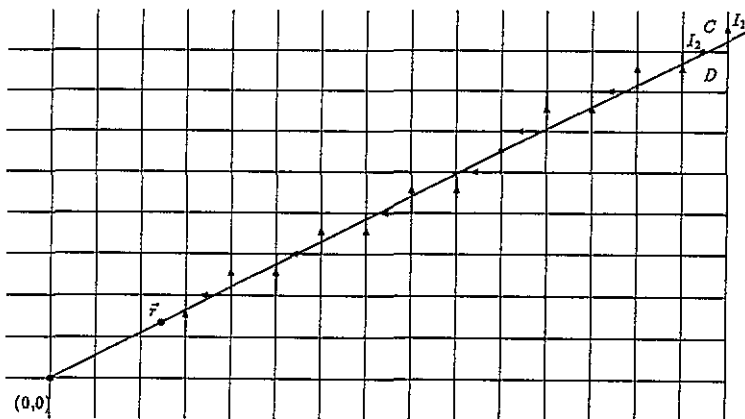

Figure A1. The link currents which contribute to the magnetization at r are shown in bold.

As will be shown below, the contribution of each link is proportional to the current along that link, in the directions indicated in figure A1. Note that after differentiation, equation (A5) reduces to

$$\sum_\sigma \hat{c}_{i\sigma}^\dagger \hat{c}_{j\sigma} \frac{iet}{\hbar} e^{\pm iA_{ij}} \frac{\delta A_{ij}}{\delta B(r)} - CC = \hat{I}_{ij} \frac{\delta A_{ij}}{\delta B(r)} \tag{A6}$$

where $\hat{I}_{ij}$ is the current operator for link $i \mapsto j$.

The functional derivative of the line integral of the vector potential, A_{ij}, is carried out using the Poincaré gauge as follows:

$$\frac{\delta}{\delta B_z(r)} \int_0^1 \lambda \, d\lambda \int_{r_i}^{r_j} B_z\left(\lambda r'\right)\left[x'dy' - y'dx'\right]$$

$$= \frac{\delta}{\delta B_z(r)} \int_0^{x_i} dx'' \int_{\lambda y_i}^{\lambda y_i + \lambda a} B_z\left(x'', y''\right) dx'' \qquad \text{(for a } y \text{ link)}$$

$$= \frac{\delta}{\delta B_z(r)} \int_0^{y_i} dy'' \int_{\lambda x_i}^{\lambda x_i + \lambda a} -B_z\left(x'', y''\right) dy'' \qquad \text{(for an } x \text{ link)} \tag{A7}$$

where a change of variable has been made: $r'' = \lambda r'$. The derivative can be taken within the integral, and the following identity used:

$$\frac{\delta B(r'')}{\delta B(r)} = \delta(r'' - r) \tag{A8}$$

which gives a contribution of unity after integration, if the position r is within the triangle created by the link $i \mapsto j$ and the origin.

Links are included right to the edge of the sample. The link current (labelled I_1) at the edge of the sample is equal to the circulating loop current around that plaquette (labelled C), which borders the sample edge. Addition of the contributing link current, labelled I_2, gives rise to the loop current around the neighbouring plaquette (labelled D). By continued use of the identity,

$$I_A^{loop} - I_B^{loop} = I_{ij} \tag{A9}$$

for loop currents circling neighbouring plaquettes, A and B, with link current I_{ij} flowing between them, the total sum of link currents indicated in figure A1 is found to be equal to the loop current around the plaquette containing r.

Hence the result follows that the magnetization at a point within a plaquette is only due to that plaquette's loop current: $M_z(r) = I_{P(r)}^{loop}$, which gives a familiar form for the magnetic moment:

$$m_z(P) = \int M(r) \cdot dS = I_P^{loop} a^2.$$

The proof can be readily generalized to any three-dimensional system with two-dimensional symmetry.

To continue then, the set of vector potentials (defined on links) must be found. Using Maxwell's equation, the induced flux per plaquette is found as

$$\int_{plaq} (\nabla \times A_{ind}(r)) \cdot dS = \mu_0 \int_{plaq} M \cdot dS \tag{A10}$$

or

$$\int_{plaq} (\nabla \times A_{ind}(r)) \cdot dS = \mu_0 I^{loop} a. \tag{A11}$$

Hence the induced flux through a plaquette is proportional to the loop current flowing around it, which means that the difference in flux between two neighbouring plaquettes is proportional to the current flowing in the link between them.

Stokes' theorem is used to obtain a set of vector potentials along links from the fluxes through plaquettes. From the identity

$$\int (\nabla \times A_{ind}(r)) \cdot dS = \oint A(r) \, dl \tag{A12}$$

one obtains for a plaquette

$$\Phi_{plaq} = \int_{plaq} (\nabla \times A_{ind}(r)) \cdot dS = \sum_{ij(plaq)} a A_{ij} \tag{A13}$$

where the final sum is around links of a plaquette in an anticlockwise direction, of the vector potentials A_{ij} attributed to the link. The arrangement is shown in figure A2. At first sight, it may seem that the vector potentials on a link will simply be proportional to the current on that link, as the sum of the former around a plaquette is proportional to the loop current around that plaquette. However, this is not the case, as the loop current around a plaquette is non-local, and dependent on all the link currents in the sample, whereas the magnetic flux through a plaquette is dependent only on the vector potentials along links local to the plaquette.
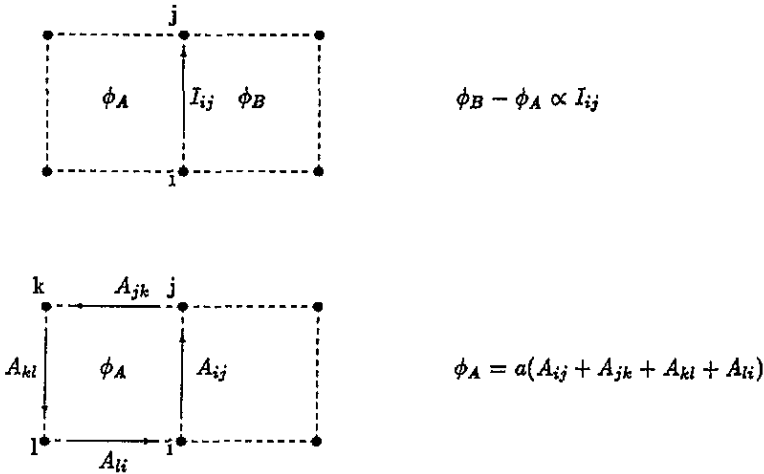

Figure A2. Currents, fields, and potentials for links and plaquettes in a discretized space.

It should be noted that the number of plaquettes is not equal to the number of links associated with any two-dimensional plane. In fact, there are two links per site, but only one plaquette, so there are twice as many link currents in a plane as loop currents, and twice as many link vector potentials as fluxes through plaquettes. The number of degrees of freedom of the link currents is halved (in a 2D problem) by the requirement of current conservation at each site. Hence apart from the overall constant, there is a one to one correspondence between link and loop currents. However, when finding a set of link vector potentials from the fluxes, constraints must be imposed in order to determine a unique set of values. These constraints are equivalent to choosing a gauge, which can be represented by a set of numbers, $\{\chi_i\}$, on each site. The constraint is that the sum of vector potentials along links to site i is equal to χ_i. The Coulomb gauge, for example, which in the continuum is given by $\nabla \cdot A(r) = 0$, becomes on a lattice the condition that $\chi_i = 0$ for all i.

Appendix B. Derivatives of eigenvalues

To take a derivative of the eigenvalue, E_λ, with respect to one of the parameters in the Hamiltonian, it is efficient to proceed as follows. Recall that

$$E_\lambda = \langle \psi_\lambda | \hat{H} | \psi_\lambda \rangle \tag{B1}$$

or

$$E_\lambda = \sum_{i,j} \left(\begin{array}{cc} u_i^{\lambda*} & v_i^{\lambda*} \end{array} \right) \left(\begin{array}{cc} H_{ij}^{(e)} & \Delta_i \delta_{ij} \\ \Delta_i^* \delta_{ij} & -H_{ij}^{(e)*} \end{array} \right) \left(\begin{array}{c} u_j^\lambda \\ v_j^\lambda \end{array} \right) \tag{B2}$$

where $H_{ij}^{(e)}$ is the normal electron Hamiltonian

$$H_{ij}^{(e)} = \left(\epsilon_0 + \frac{U n_i}{2} - \mu \right) + t_{ij}. \tag{B3}$$

Hence taking the derivatives, we have for example

$$\frac{\partial E_\lambda}{\partial \mu} = \sum_i \left(\begin{array}{cc} u_i^{\lambda*} & v_i^{\lambda*} \end{array} \right) \left(\begin{array}{cc} -1 & 0 \\ 0 & 1 \end{array} \right) \left(\begin{array}{c} u_i^\lambda \\ v_i^\lambda \end{array} \right) = -\sum_i \left(|u_i^\lambda|^2 - |v_i^\lambda|^2 \right) \tag{B4}$$

and

$$\frac{\partial E_\lambda}{\partial \Delta_i} = \left(\begin{array}{cc} u_i^{\lambda*} & v_i^{\lambda*} \end{array} \right) \left(\begin{array}{cc} 0 & 1 \\ 0 & 0 \end{array} \right) \left(\begin{array}{c} u_i^\lambda \\ v_i^\lambda \end{array} \right) = u_i^{\lambda*} v_i^\lambda \tag{B5}$$

which are the identities required in section 4.

Appendix C. The semiclassical approximation

A semiclassical argument can be followed to produce an approximate form for the energy spectrum of a superconductor in the vortex state. To simplify matters, we drop the periodic potential and develop the method for the continuum Bogoliubov–de Gennes equation

$$\left(\begin{array}{cc} \hat{H}(r) & \Delta(r) \\ \Delta^*(r) & -\hat{H}^*(r) \end{array} \right) \left(\begin{array}{c} u^\lambda(r) \\ v^\lambda(r) \end{array} \right) = E_\lambda \left(\begin{array}{c} u^\lambda(r) \\ v^\lambda(r) \end{array} \right) \tag{C1}$$

where $\hat{H}(r)$ is the one-electron Hamiltonian with no external potential, and $\Delta(r)$ is a given pairing potential. We generalize the usual semiclassical theory by assuming that the solution of equation (C1) takes the following form:

$$\left(\begin{array}{c} u^\lambda(r) \\ v^\lambda(r) \end{array} \right) = e^{\frac{i}{\hbar} \left[S(r)\underline{1} + \Sigma(r)\underline{\tau}_z \right]} \left(\begin{array}{c} \bar{u} \\ \bar{v} \end{array} \right) \tag{C2}$$

where the real functions S, Σ, $\bar{u}$ and $\bar{v}$ are slowly varying functions of r. Substituting equation (C2) into equation (C1), to lowest order in $\hbar$ we find that the quasiparticle energy eigenvalue, E, is given by

$$E = \frac{1}{m} \nabla S \cdot (\nabla \Sigma - eA) \pm \sqrt{\left\{ \frac{1}{2m} \left[|\nabla S|^2 + (\nabla \Sigma - eA)^2 \right] - \mu \right\}^2 + |\Delta|^2} \tag{C3}$$

where the phase $\Sigma(r)$ is determined by the phase of

$$\Delta(r) = |\Delta(r)| \, e^{i\phi(r)} \tag{C4}$$

via the condition $\phi + (2/\hbar)\Sigma = $ an integer. As usual, at this stage one must find the family of orbits in phase space, $(\nabla S(r), r)$, such that E in equation (C3) is a constant and select

from these the orbits for which the wavefunction in equation (C2) is single valued, namely, those satisfying the conditions

$$\frac{1}{\hbar} \oint \nabla S \cdot \mathrm{d}r = \pi n_a$$

and

$$\frac{1}{\hbar} \oint \nabla \Sigma \cdot \mathrm{d}r = \pi n_b$$

for n_a and n_b integers, either both odd or both even. Note that while the sum and difference of the phase integrals (appropriate to either an electron or hole) lead to the usual quantization condition of $2n\pi$, individually each one has half the normal quantization, which is essential to give the appropriate quantization for Cooper pairs.

We continue by making use of equation (C3) to make a simple estimate of E. To do this we neglect all the complexities introduced by the amplitude variations of $\Delta(r)$ and $B(r)$ with r due to the Abrikosov flux lattice, and replace them by constants, $|\Delta|$ and B. Then by neglecting the cross-term, $\nabla S \cdot (\nabla \Sigma - eA)$, and in the Landau gauge, $A = -yB\hat{e}_x$, we find that the energy spectrum becomes

$$E = \pm \sqrt{\left\{ \frac{1}{2m} \left[\left(\frac{\mathrm{d}S}{\mathrm{d}y} \pm \frac{\mathrm{d}\Sigma}{\mathrm{d}y} \right)^2 + (eB)^2 (y - y_0)^2 \right] - \mu \right\}^2 + |\Delta|^2}. \quad (C5)$$

The above equation (C5) contains the form of a simple harmonic oscillator, with $\mathrm{d}S/\mathrm{d}y \pm \mathrm{d}\Sigma/\mathrm{d}y$ playing the role of the momentum, P, conjugate to a coordinate variable, $Q = eB(y - y_0)$. This implies that the conditions

$$\frac{1}{\hbar} \oint \mathrm{d}r \cdot (\nabla S(r) \pm \nabla \Sigma(r)) = 2\pi n \quad (C6)$$

reduce to the Bohr–Sommerfeld quantization condition as

$$\oint P \, \mathrm{d}Q = 2\pi n \hbar e B \quad (C7)$$

and the quasiparticle energy is quantized as follows:

$$E_n = \pm \sqrt{\left[\hbar \omega_c (n + 1/2) - \mu \right]^2 + |\Delta|^2} \quad (C8)$$

where $\omega_c = eB/m$. Clearly, this spectrum of Landau levels shifted into two square root singularities, with a gap between them, is qualitatively similar to the exact solution described by figure 9(a) (except without states in the gap due to normal regions).

References

[1] Abrikosov A A 1957 *Sov. Phys.–JETP* **5** 1174; 1957 *Zh. Eksp. Teor. Fiz.* **32** 1442
[2] Rasolt M and Tešanović Z 1992 *Rev. Mod. Phys.* **64** 709
[3] Norman M, Akera H and MacDonald A H 1992 *Physica* C **196** 43
[4] Maniv T, Rom A I, Markiewicz R S, Vagner I D and Wyder P 1991 *J. Phys. Chem. Solids* **52** 1391
[5] Maniv T, Rom A I, Vagner I D and Wyder P 1992 *Phys. Rev.* B **40** 8360
[6] Dukan S, Andreev A V and Tešanović Z 1991 *Physica* C **183** 355
[7] Graebner J E and Robbins M 1976 *Phys. Rev. Lett.* **36** 422
[8] Harrison N, Hayden S M, Meeson P, Springford M, van der Wel P J and Menovsky A A 1994 *Phys. Rev.* B **70** 4208
[9] Corcoran R, Harrison N, Hayden S M, Meeson P, Springford M and van der Wel P J 1994 *Phys. Rev. Lett.* **52** 701

[10] Corcoran R, Meeson P, Onuki Y, Probst P-A, Springford M, Takita K, Harima H, Guo G Y and Györffy B L 1994 *J. Phys.: Condens. Matter.* **6** 4479

[11] Györffy B L, Staunton J B and Stocks G M 1991 *Phys. Rev.* B **44** 5190

[12] Haydock R 1980 *Solid State Physics* vol 35 (New York: Academic)

[13] 1984 *The Recursion Method and Its Applications (Springer Series in Solid State Sciences 58)* (Berlin: Springer)

[14] Haydock R, Heine V and Kelly M J 1975 *J. Phys. C: Solid State Phys.* **8** 2591

[15] Litak G, Miller P and Györffy B L 1992 to be published

[16] Nicholson D M and Stocks G M private communication

[17] Press W H, Teukolsky S A, Vetterling W T and Flannery B P (ed) *Numerical Recipes in Fortran* 2nd edn (Cambridge: Cambridge University Press)

[18] Caroli C, de Gennes P G and Matricon J 1964 *Phys. Lett.* **9** 307

[19] Eilenberger G and Büttner H 1969 *Z. Phys.* **224** 335

[20] Gygi F and Schluter M 1990 *Phys. Rev.* B **41** 822

[21] de Gennes P G 1966 *Superconductivity of Metals and Alloys* (Reading, MA: Addison-Wesley)

[22] Mathews J and Walker R L 1970 *Mathematical Methods of Physics* (Reading, MA: Addison-Wesley)

[23] Bardeen J, Jacobs A E, Kümmel R and Tewordt L 1969 *Phys. Rev.* **187** 556

[24] Pöttinger B and Klein U 1993 *Phys. Rev. Lett.* **70** 2806

[25] Pippard A B 1967 *Solid State Physics* vol 1 (London: Gordon and Breach)

[26] Callaway D J E 1993 *Ann. Phys., NY* **224** 210

[27] Kogan V G 1975 *J. Low Temp. Phys.* **20** 103

[28] Abrikosov A A 1988 *Fundamentals of the Theory of Metals* (Amsterdam: North-Holland)

[29] Canel E 1965 *Phys. Lett.* **16** 101

[30] Hofstadter D R 1976 *Phys. Rev.* B **14** 2239

[31] Lifshitz E M and Kosevich L P 1980 *Landau and Lifshitz Course of Theoretical Physics, Vol 9—Statistical Physics Part 2 (Section 63)* (Pergamon)

[32] Miller P and Györffy B L 1995 *Phys. Rev. Lett.* at press

[33] Miyake K 1993 *Physica* B **186** 115

[34] Maki K 1991 *Phys. Rev.* B **44** 2861

[35] Kittel C 1976 *Introduction to Solid State Physics* 5th edn (New York: Wiley) ch 9

[36] Dang E K F 1992 *PhD Thesis* Bristol University

[37] Brittin W E, Smythe W R and Wyss W 1982 *Am. J. Phys.* **50** 693